Syntheses, Characterization, and Properties of Vanadium(III) Complexes Containing Tripodal Tetradentate Ligands with Single Pyridyl Groups

Kan Kanamori,* Eiji Kameda, Takatsugu Kabetani, Taiko Suemoto, Ken-ichi Okamoto,† and Sumio Kaizaki††

Department of Chemistry, Faculty of Science, Toyama University, Gofuku 3190, Toyama 930

†Department of Chemistry, University of Tsukuba, Tsukuba, Ibaraki 305

††Department of Chemistry, Faculty of Science, Osaka University, Toyonaka, Osaka 560

(Received April 26, 1995)

The syntheses, characterization, and properties of $[V(pda)(OH)(H_2O)]$ (**1a**), $[V_2(\mu\text{-}O)(pda)_2(H_2O)_2]$ (**1b**), $[V_2(\mu\text{-}O)(bpg)_2Br_2]$ (**2**); and $[V_2(\mu\text{-}O)Br_2(tpa)_2]Br_2$ (**3**) are described, where pda (*N*-(2-pyridylmethyl)-iminodiacetate), bpg (*N*,*N*-bis(2-pyridylmethyl)glycinate), and tpa (tris(2-pyridylmethyl)amine) are tripodal tetradentate ligands with single pyridyl groups. Complexes **1a**, **1b**, and **2** were characterized on the basis of their electronic and Raman spectra. The structure of **3** was determined by X-ray crystallography. Complex **3** crystallizes in the $P\bar{1}$ space group with the following unit cell dimensions: a=11.505(5), b=11.509(5), c=16.348(7) Å, α=103.73(2)°, β=103.71(2)°, γ=93.26(3)°, and Z=2. The V–O–V angle is 175.3(2)° and the V–μ-O distances are 1.783(2) and 1.784(2) Å. In complex **3**, the four unpaired electrons are ferromagnetically coupled. It was found that there is a positive correlation between $2 \times \nu_{as}$(V–O–V) and the energy of the oxo-to-V(III) charge-transfer transition for single oxo-bridged dinuclear vanadium(III) complexes including the present complexes. This correlation is discussed in terms of the π character of the V(III)–μ-O bond that is affected by the remaining donor groups.

It is well-known that certain ascidians sequester vanadium(III) in their blood cells.[1,2] Recently the fan worm, *Pseudopotamilla occelata*, was found to be a new vanadium(III) accumulator in the Animal Kingdom.[3] With regard to the vanadium(III) in ascidians, its coordination environment is still a controversial issue even at the present time when more than 80 years have passed from the original finding by Henze.[4] The chemical formula of the vanadium(III) ion in the fan worm has also not been clarified.

Several types of oxo-bridged dinuclear iron(III) units have been found in the invertebrate dioxygen carrier, hemerythrine, and in the enzymes ribonucleotide reductase, purple acid phosphatase, and methane mono oxygenase. Oxo-bridged species of manganese have also been investigated widely in relation to the metal center of photosystem II (PSII) in green plants. The so-called "Henze's solution (vanadocyte hemolysate)" exhibits an intense absorption band near 450 nm that can be attributed to an oxo-bridged dinuclear vanadium(III) complex.[5—7]

The oxo-bridged iron(III)–pda complexes with an additional carbonato[8] or an acetato bridge[9] have recently been reported. An oxo-bridge has also been found in the mixed-valence dinuclear vanadium(IV,V) complex containing a pda analog, [[1-(2-pyridyl)ethyl]imino]diacetate.[10] An iron(III) complex with bpg has been investigated with regard to nonheme iron oxygenases.[9] A di(μ-oxo) mixed-valence manganese(III,IV) complex with bpg ligands has been structurally characterized.[11] The oxo-bridged dinuclear iron and manganese complexes with tpa have been extensively studied.[12] However, few studies have been done on oxo-bridged dinuclear vanadium(III) complexes containing pda, bpg, or tpa.

Considering that oxo-bridged dinuclear iron and manganese complexes play important roles in biochemical reactions, the oxo-bridged vanadium(III) unit may likely be one of the candidates for the active form of vanadium(III) in vanadium accumulators such as ascidians and fan worms. In this report, we are concerned with the oxo-bridged dinuclear vanadium(III) complexes containing tripodal tetradentate ligands with single pyridylmethyl groups such as pda, bpg, and tpa.

Experimental

Preparation of Ligands. Tris(2-pyridylmethyl)-amine (tpa) was synthesized according to the literature procedures.[13] *N*-(2-pyridylmethyl)iminodiacetate (pda) and *N*,*N*-bis(2-pyridylmethyl)glycinate (bpg) were also prepared

and isolated as their acid forms as in the literature,[14] but these ligands can be isolated more conveniently as lithium and barium salts.

Li_2pda. A solution of $LiOH \cdot H_2O$ (8.2 g; 0.2 mol) in 80 cm^3 of H_2O was added slowly to a solution of monochloroacetic acid (18.9 g; 0.2 mol) in 20 cm^3 of H_2O below 5 °C. After neat 2-aminomethylpyridine (10.8 g; 0.1 mol) was added dropwise to the above solution at 30 °C, a solution of $LiOH \cdot H_2O$ (8.2 g; 0.2 mol) dissolved in 80 cm^3 of water was added dropwise to the mixture keeping the pH of the solution at 10—11. The resulting solution was stirred at 40 °C overnight. The solution was then evaporated to 50 cm^3 on a water bath. This concentrated solution was cooled and ethanol was added to obtain Li_2pda as a white mass. The crude product was recrystallized from hot water. Yield: 17 g (63%). Anal. Calcd for $C_{10}H_{14}N_2O_6Li_2$: C, 44.14; H, 5.18; N, 10.30%. Found: C, 44.04; H, 5.10; N, 10.23%.

Bapda. A solution of $Li_2pda \cdot 2H_2O$ (35.3 g; 0.13 mol) in 200 cm^3 of water was mixed with a solution of $BaCl_2 \cdot 2H_2O$ (31.7 g; 0.13 mol) in 150 cm^3 of water. The resulting insoluble barium salt of pda^{2-} was filtered, washed with water, and air-dried. Yield: 51 g (99%).

Libpg. Glycine (1.14 g; 15.25 mmol) in 10 cm^3 of H_2O was neutralized with a solution of $LiOH \cdot H_2O$ (0.68 g; 15.25 mmol). The solution was combined with an aqueous ethanol (1 : 3) solution (40 cm^3) of 2-picolyl chloride hydrochloride (5.0 g; 30.5 mmol) previously neutralized with $LiOH \cdot H_2O$ (1.28 g; 30.5 mmol). An aqueous solution (10 cm^3) of $LiOH \cdot H_2O$ (1.28 g; 30.5 mmol) was added slowly to this solution keeping the pH of the solution at 10—11. The resulting mixture was stirred at room temperature overnight. The solution was then evaporated to give a white precipitate. The crude product was filtered off and recrystallized from hot ethanol. Yield: 2.1 g (70%). Anal. Calcd for $C_{14}H_{18}N_3O_4Li$: C, 56.24; H, 6.07; N, 14.05%. Found: C, 56.18; H, 6.04; N, 13.61%.

Preparation of Complexes. All manipulation was carried out under argon atmosphere using standard Schlenk techniques or in a nitrogen-filled dry box. Argon was purified by passage through a gas-purification column (Gasclean, Nikka Seiko Co.) before use.

$[V(pda)(OH)(H_2O)]$ (1a). $V_2(SO_4)_3$ (2.0 g; 5 mmol) was suspended in 30 cm^3 of water. Solid $BaBr_2 \cdot 2H_2O$ (1.7 g; 5 mmol) was added to the suspension and the resultant mixture was stirred at 50 °C for a day. The precipitated barium sulfate was removed by filtration. To the VBr_3 solution thus obtained was added a solution of $Li_2pda \cdot 2H_2O$ (2.7 g; 10 mmol) in 40 cm^3 of water. The resulting solution was evaporated to dryness and the residue was dissolved in a small amount of water. Ethanol (20 cm^3) was added to the solution, then a green precipitate was obtained by cooling it at 5 °C. The precipitate was collected by filtration and recrystallized from aqueous ethanol. Yield: 0.85 g (28%). Anal. Calcd for $C_{10}H_{13}N_2O_6V$: C, 39.00; H, 4.25; N, 9.10%. Found: C, 38.81; H, 4.47; N, 8.91%.

$[V_2(\mu\text{-}O)(pda)_2(H_2O)_2] \cdot H_2O \cdot 0.5KBr$ (1b). To a suspension containing $Bapda \cdot 2H_2O$ (3.95 g; 10 mmol) and $BaBr_2 \cdot 2H_2O$ (1.33 g; 5 mmol) was added a solution of $V_2(SO_4)_3$ (1.95 g; 5 mmol) in 30 cm^3 of water. The suspension was stirred overnight. A solution of K_2CO_3 (0.69 g; 5 mmol) in 20 cm^3 of water was added to the suspension and the mixture was stirred for 3 h. The precipitated barium sulfate was filtered off. The volume of the filtrate was reduced by half and this solution was kept standing at room temperature for 1—3 weeks. Brown columnar crystals deposited and were collected by filtration. Yield: 0.1 g (3%) Anal. Calcd for $C_{20}H_{26}N_4O_{12}Br_{0.5}K_{0.5}V_2$: C, 35.54; H, 3.89; N, 8.29%. Found: C, 35.51; H, 4.00; N, 8.21%.

$[V_2(\mu\text{-}O)(bpg)_2Br_2] \cdot 5H_2O \cdot LiBr$ (2). An aqueous solution of VBr_3 was obtained from double decomposition of $V_2(SO_4)_3$ (0.39 g; 1.0 mmol) with $BaBr_2 \cdot 2H_2O$ (1.0 g; 3.0 mmol) in a manner similar to that described above. The solution was evaporated to dryness and the green residue was dissolved in 20 cm^3 of methanol. The solution was then mixed with a solution of $Libpg \cdot 2H_2O$ (0.60 g; 2 mmol) in 20 cm^3 of methanol. The reaction mixture was evaporated to dryness. The residue and $LiBr \cdot H_2O$ (2.08 g; 20 mmol) was dissolved in a small amount of methanol. To the solution was added 40 cm^3 of acetone and the mixture was kept at 65 °C. Purple-brown crystals formed and were collected by filtration. Yield: 0.52 g (54%). Anal. Calcd for $C_{28}H_{38}N_6O_{10}Br_3LiV_2$: C, 34.77; H, 3.97; N, 8.69%. Found: C, 34.85; H, 3.90; N, 8.64%.

$[V_2(\mu\text{-}O)(tpa)_2Br_2]Br_2 \cdot 2H_2O$ (3). A solution of tpa (1.00 g; 3.44 mmol) dissolved in a small amount of methanol was mixed with a methanol solution (15 cm^3) of VBr_3 obtained from $V_2(SO_4)_3$ (0.68 g; 1.7 mmol) and $BaBr_2 \cdot 2H_2O$ (1.72 g; 5.2 mmol). The mixture was warmed at 50 °C to give a purple solution. To the resulting purple solution was added a 2× volume of acetone and the mixture was kept at 50 °C. Purple crystals deposited and were collected by filtration and dried in air. Yield: 1.1 g (61%). Anal. Calcd for $C_{36}H_{40}N_8O_3Br_4V_2$: C, 41.01; H, 3.82; N, 10.63%. Found: C, 40.95; H, 3.76; N, 10.47%.

Measurements. Raman spectra were recorded on a JASCO R-800 laser Raman spectrophotometer with excitation by an Ar^+-ion laser line, 514.5 nm. Solid samples for the Raman measurements were formed into KBr disks.[15] UV-vis spectra were measured using a JASCO Ubest 50 spectrophotometer. Diffuse reflectance spectra were obtained for complexes diluted with MgO. Magnetic susceptibility was measured by a PAR-4500 vibrating sample magnetometer (VSM) in the temperature range of 1.6 to 300 K.

X-Ray Structure Determination. Crystallographic data are summarized in Table 1. A crystal of $[V_2(\mu\text{-}O)(tpa)_2Br_2]Br_2 \cdot 2H_2O$ was mounted on a glass fiber, coated with epoxy as a precaution against solvent loss, and centered on an Enraf–Nonius CAD4 diffractometer using graphite-monochromated Mo $K\alpha$ radiation. Unit cell parameters were determined by a least-squares refinement, using the setting angles of 25 reflections in the range of $16 < 2\theta < 20°$. Data reduction and application of Lorentz, polarization, linear decay correction (correction factor on I, 1.000 to 1.000), and empirical absorption corrections based on a series of psi scans (min and max transmission factors, 0.88 to 1.00) were carried out using the Enraf–Nonius Structure Determination Package.[16]

The structure was solved by a direct method[16] and conventional difference Fourier techniques. The structure was refined by full-matrix least-squares techniques. All non-hydrogen atoms were refined anisotropically. All the calculations were done on a VAX computer using the crystallographic package MOLEN.[17] Non-hydrogen atom coordinates are listed in Table 2. Lists of bond lengths and bond

Table 1. Crystallographic Data for $[V_2OBr_2(tpa)_2]Br_2 \cdot 2H_2O$

Formula	$C_{36}H_{40}N_8Br_4O_3V_2$	Z	2
Fw	1054.29	$\rho_{calc}/g\,cm^{-3}$	1.72
Crystal size/mm^3	0.45×0.45×0.50	$F(000)$	1044
Crystal system	Triclinic	$\lambda(Mo\,K\alpha)/Å$	0.71073
Space group	$P\bar{1}$	$\mu(Mo\,K\alpha)/cm^{-1}$	43.9
a/Å	11.505(5)	2θ	$\leq 50°$
b/Å	11.509(5)	Reflections:	
c/Å	16.348(7)	Measured	7410
α/degree	103.73(2)	Independent	7131
β/degree	103.71(2)	$F_o > 3\sigma(F_o)$	5947
γ/degree	93.26(3)	R[a)]	0.031
T/K	300	R_w[a)]	0.030
V/Å^3	2028(1)		

a) $R=\Sigma||F_o|-|F_c||/\Sigma|F_o|$, $R_w=[\Sigma w(|F_o|-|F_c|)^2/\Sigma w|F_o|^2]^{1/2}$.

angles, anisotropic thermal parameters, hydrogen atom positions, and F_o-F_c tables were deposited as Document No. 68047 at the Office of the Editor of Bull. Chem. Soc. Jpn.

Results and Discussion

Figure 1 depicts the tripodal ligands with pyridylmethyl groups employed in this study, along with the structurally-related ligand, nta (nitrilotriacetate). We have shown that nta yields a heptacoordinate vanadium(III) complex and that hydrolysis of this complex does not give an oxo-bridged dinuclear complex.[15,18] On the other hand, hexacoordinate aminopolycarboxylato vanadium(III) complexes such as [V(1,3-pdta)]$^-$ (1,3-pdta; 1,3-diaminopropane-*N*,*N*,*N*′,*N*′-tetraacetate) yield oxo-bridged dinuclear complexes on base-hydrolysis.[15] It is, therefore, of interest to examine first whether the replacement of an nta acetate group by a methylpyridyl group would change the coordination structure of the vanadium(III) complex and, as a result, the properties concerning the oxo-bridged dimer formation.

pda Complex. In the present study, green and brown vanadium(III) complexes containing one pda ligand per vanadium(III) atom were isolated. The Raman spectrum of the solid green pda complex does not exhibit any band characteristic of a μ-oxo species. The diffuse reflectance spectrum exhibits no pronounced bands in the 800 nm region that are diagnostic of heptacoordinate vanadium(III) complexes.[19] These observations indicate that the green complex is a monomeric hexacoordinate complex that can be formulated as [V(pda)(OH)(H_2O)] based on elemental analysis. Although a μ-dihydroxo dimeric structure can alternatively explain the elemental analysis, the above conclusion would be more reasonable since μ-dihydroxo-bridged vanadium(III) complexes have not been identified so far.

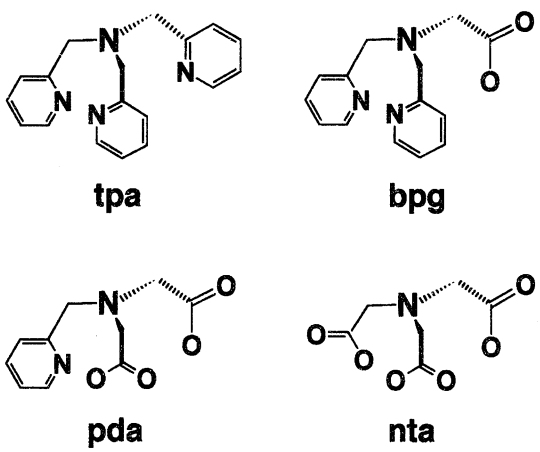

Fig. 1. Tripodal tetradentate ligands.

It is of interest to note that though both the pda and nta ligands form only five-membered chelate rings on coordination, the pda complex adopts a hexacoordinate structure while the nta complex forms a heptacoordinate structure.[18] Since no significant differences are expected in the distances and bite angles of the nta and pda chelate-ring systems, the difference in the coordination geometry between the nta and pda complexes must result from the differences in the ligand-field strengths of the coordinated carboxylate oxygen atom and the pyridyl nitrogen atom.

It can be reasonably argued that whether a vanadium(III) complex adopts a hexacoordinate structure or a heptacoordinate one depends on the balance between the energy gain due to ligand-field stabilization and the energy loss due to the strain caused by coordination of a multidentate ligand in a restricted arrangement. The regular octahedral structure should be the most favorable one for vanadium(III) to obtain a maximal ligand-field stabilization energy. On the other hand, a tripodal tetradentate ligand such as nta or pda experiences a rather large strain energy when it coordinates to a metal center and adapts an octahedral geometry. Thus, it can be predicted that a weak-field chelate such as nta prefers a less-strained heptacoordinate structure, since the loss of the ligand-field stabilization energy caused by a deviation from the regular octahedral geometry would be small. Conversely, for a stronger-field chelate such as pda, the ligand field-stabi-

lization energy would surpass the strain energy within the ligand chelated in an octahedral fashion, resulting in a hexacoodinate structure.

Table 2. Final Atomic Coordinates and Equivalent Isotropic Thermal Parameters (B_{eq}/Å^2) for Non-Hydrogen Atoms of $[V_2OBr_2(tpa)_2]Br_2 \cdot 2H_2O$ ($B_{eq}=(8\pi^2/3)\Sigma\Sigma U_{ij} a_i^* a_j^* \boldsymbol{a}_i \cdot \boldsymbol{a}_j$)

Atom	x	y	z	B_{eq}
Br1	0.78791(4)	0.48941(4)	0.44846(2)	3.410(9)
Br2	0.51056(4)	0.21213(4)	0.05153(2)	3.427(9)
Br3	0.70347(5)	0.90852(4)	0.49932(3)	4.40(1)
Br4	1.09151(4)	0.29656(5)	0.00066(3)	4.41(1)
V1	0.78790(5)	0.45230(5)	0.29058(3)	1.84(1)
V2	0.54761(5)	0.21209(5)	0.20934(3)	1.84(1)
O	0.6721(2)	0.3279(2)	0.2500(1)	1.88(5)
Ow1	0.8343(4)	0.4045(3)	−0.0786(3)	6.0(1)
Ow2	0.4036(4)	0.8346(4)	0.4212(3)	6.2(1)
N1	0.8323(3)	0.4451(3)	0.1701(2)	2.20(6)
N2	0.5546(3)	0.1677(3)	0.3300(2)	2.27(6)
N11	0.9259(3)	0.3365(3)	0.2925(2)	2.41(6)
N21	0.9218(3)	0.6124(3)	0.3252(2)	2.62(7)
N31	0.6693(3)	0.5694(3)	0.2438(2)	2.32(6)
N41	0.6632(3)	0.0738(3)	0.2074(2)	2.42(6)
N51	0.3878(3)	0.0782(3)	0.1747(2)	2.62(7)
N61	0.4302(3)	0.3303(3)	0.2564(2)	2.21(6)
C11	0.8531(3)	0.3179(3)	0.1384(2)	2.50(7)
C12	0.9366(3)	0.2830(3)	0.2119(2)	2.66(8)
C13	1.0192(4)	0.2031(4)	0.1995(3)	4.4(1)
C14	1.0914(4)	0.1778(5)	0.2723(4)	5.5(1)
C15	1.0803(4)	0.2302(5)	0.3532(3)	4.8(1)
C16	0.9979(4)	0.3098(4)	0.3616(3)	3.39(9)
C21	0.9453(4)	0.5244(4)	0.1809(3)	3.34(9)
C22	0.9801(3)	0.6204(3)	0.2644(2)	2.53(7)
C23	1.0695(4)	0.7134(4)	0.2777(3)	3.64(9)
C24	1.0974(4)	0.8031(4)	0.3542(3)	4.6(1)
C25	1.0347(5)	0.7978(4)	0.4150(3)	4.7(1)
C26	0.9480(4)	0.7024(4)	0.3989(3)	3.6(1)
C31	0.7254(4)	0.4772(4)	0.1110(2)	3.05(8)
C32	0.6576(3)	0.5641(3)	0.1592(2)	2.59(8)
C33	0.5799(5)	0.6307(4)	0.1169(3)	4.5(1)
C34	0.5113(5)	0.7011(4)	0.1613(3)	5.6(1)
C35	0.5228(4)	0.7069(4)	0.2473(3)	4.6(1)
C36	0.6032(4)	0.6413(4)	0.2868(3)	3.18(9)
C41	0.6823(3)	0.1468(3)	0.3616(2)	2.46(7)
C42	0.7168(3)	0.0633(3)	0.2878(2)	2.63(8)
C43	0.7959(4)	−0.0198(4)	0.2993(3)	4.4(1)
C44	0.8227(5)	−0.0918(5)	0.2275(4)	5.8(1)
C45	0.7702(5)	−0.0807(4)	0.1462(3)	4.7(1)
C46	0.6908(4)	0.0020(4)	0.1382(3)	3.32(9)
C51	0.4753(4)	0.0551(3)	0.3188(2)	3.20(8)
C52	0.3796(3)	0.0204(3)	0.2357(2)	2.55(7)
C53	0.2860(4)	−0.0705(4)	0.2219(3)	3.7(1)
C54	0.1966(4)	−0.0966(4)	0.1455(3)	4.5(1)
C55	0.2027(4)	−0.0347(5)	0.0852(3)	4.6(1)
C56	0.2975(4)	0.0518(4)	0.1011(3)	3.8(1)
C61	0.5221(4)	0.2737(4)	0.3891(2)	3.12(8)
C62	0.4349(3)	0.3420(3)	0.3410(2)	2.60(8)
C63	0.3694(4)	0.4196(5)	0.3833(3)	4.5(1)
C64	0.2988(4)	0.4879(5)	0.3388(3)	5.5(1)
C65	0.2921(4)	0.4762(4)	0.2528(3)	4.4(1)
C66	0.3588(4)	0.3964(4)	0.2129(3)	3.18(9)

The solution behavior of the green pda complex was examined using visible absorption and resonance Raman spectra. Figure 2 displays the absorption spectra of the green pda complex ($[V^{3+}]$=16 mM) (1 M=1 mol dm^{-3}) as a function of pH. The 460-nm band grows with increasing solution pH, and the color of the solution turns from brownish green to dark brown. This pH dependence of the absorption spectrum is similar to those observed for the oxo-bridged dimer formation of aqua[20] and aminopolycarboxylato[15] vanadium(III) complexes.

The formation of an oxo-bridged pda complex by hydrolysis was ascertained by Raman measurements. Figure 3-B depicts the Raman spectrum of a solution of the green pda complex at pH 5.0. The observed features are typical of the resonance Raman spectrum of the oxo-

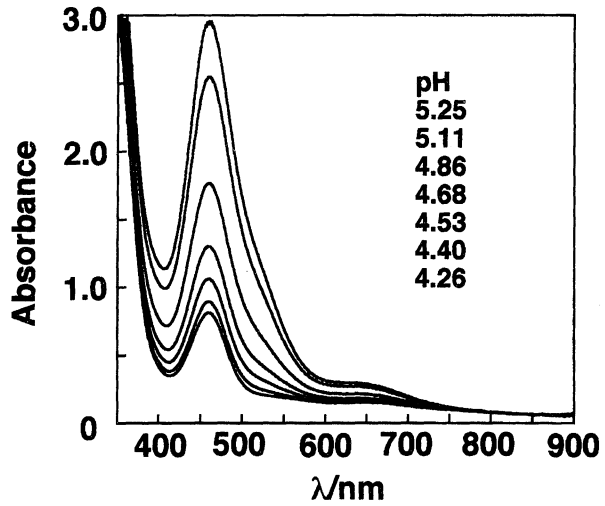

Fig. 2. Absorption spectra of [V(pda)(OH)(H_2O)] in aqueous solution (18 mM) as a function of pH.

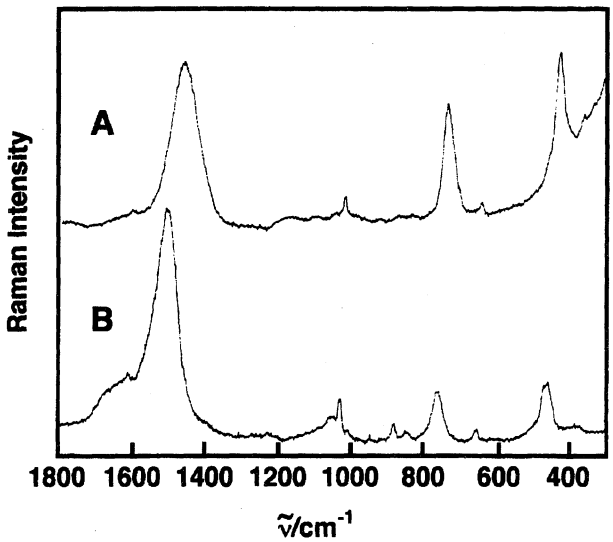

Fig. 3. Raman spectra of the vanadium(III)–pda complexes: A, aqueous solution of the green pda complex (18 mM, pH 5); B, solid sample of the brown pda complex.

bridged dinuclear vanadium(III) complexes.[15,20,21] The 760 and 458 cm^{-1} bands are, then, assignable to the antisymmetric (ν_{as}) and symmetric (ν_s) V–O–V stretching vibrations, respectively. (The 470 cm^{-1} band is also in the region of the symmetric V–O–V stretching vibration, but we assigned it to an internal mode of the pyridyl group[22] by comparing the spectrum with that obtained for the solid sample.) The most intense band at 1504 cm^{-1} is assigned to the overtone of the antisymmetric V–O–V stretching vibration. This strongly resonance-enhanced overtone of ν_{as}(V–O–V) is the most pronounced resonance Raman characteristic to the oxo-bridged dinuclear vanadium(III) complexes. The oxo-bridged dinuclear vanadium(III)–pda complex was isolated as brown crystals, though the yield was very poor. The Raman spectrum of the solid brown complex is shown in Fig. 3-B. Although the vibrational wavenumbers due to the V–O–V moiety observed for the solid sample (443, 749, and 1472 cm^{-1}) are slightly shifted to a lower energy compared to those observed for the solution sample, it is recognized that the dinuclear vanadium(III) complex with pda takes a similar bridging mode both in solution and the solid state.

bpg Complex. Figure 4 illustrates the diffuse reflectance (A) and absorption (B) spectra of the bpg vanadium(III) complex. The absorption spectral features are typical of oxo-bridged dinuclear vanadium(III). The LMCT band, which maximizes at 528 nm for the solid sample, shifts to 480 nm for the solution sample. This shift would be explained in terms of an aquation of the bromo complex in water;

$$[V_2(\mu\text{-O})(bpg)_2Br_2] + 2H_2O \longrightarrow [V_2(\mu\text{-O})(bpg)_2(OH_2)_2]^{2+} + 2Br^-.$$

Figure 5 shows the resonance Raman spectra of the bpg complex in the solid state (A) and in aqueous solution (B). The strongly resonance-enhanced Raman band due to $2\times\nu_{as}$(V–O–V) verifies the oxo-bridged structure of the bpg complex. It is noteworthy that on the aquation of $[V_2(\mu\text{-O})(bpg)_2Br_2]$ $2\times\nu_{as}$(V–O–V) shifts to a higher energy as observed for the LMCT band. This shift of the resonance Raman band associated with the LMCT band will be discussed later in detail.

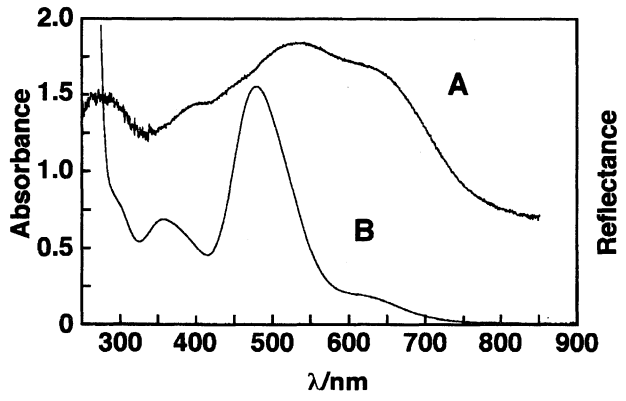

Fig. 4. Reflectance (A) and absorption (B) spectra of $[V_2(\mu\text{-O})(bpg)_2Br_2]$.

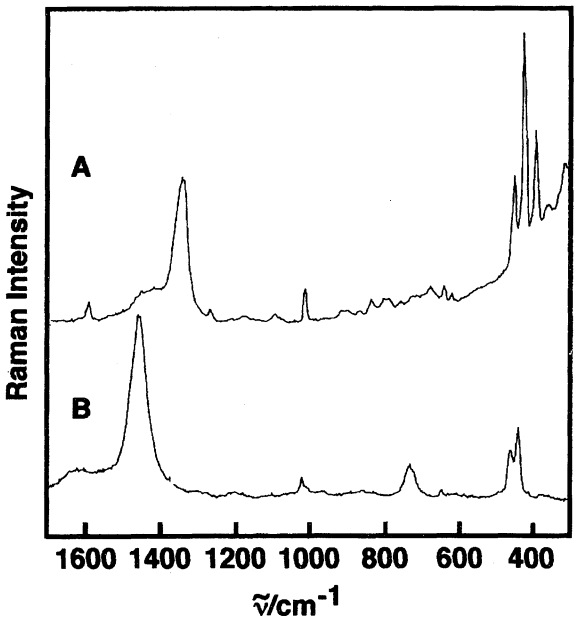

Fig. 5. Raman spectra of $[V_2(\mu\text{-O})(bpg)_2Br_2]$: A, solid state; B, aqueous solution.

There is some difference in the dimerization tendency between the pda and the bpg complexes. In fact, a 0.5 mM solution of the bpg complex shows a pronounced LMCT band due to the oxo-bridged dimer down to pH 2.61, whereas a 3 mM solution of the pda complex shows only a weak LMCT band even at pH 4.26. This observation indicates that the dimerization tendency of the bpg complex is larger than that of the pda complex. The higher dimerization tendency of the bpg complex compared to the pda complex can be explained by considering the net charge of the respective vanadium(III) complexes. Namely, substitution of an anionic carboxylate group by a neutral pyridyl group in a tetradentate ligand increases the net positive charge on the vanadium(III) complex, being more favorable for the deprotonation of an aqua ligand to yield an oxo-bridged dimer.

tpa Complex. The structure of the vanadium(III)–tpa complex obtained in the present work was crystallographically characterized. A perspective view of the complex cation is shown in Fig. 6 and selected bond lengths and angles are summarized in Table 3. The X-ray analysis reveals that complex **3** is an oxo-bridged dinuclear vanadium(III) complex. The two monomeric units are arranged nearly centrosymmetrically. This geometrical arrangement is similar to those found in $[Cr_2(\mu\text{-O})(NCS)_2(tpa)_2]^{2+}$,[23] $[V_2O_2(\mu\text{-O})(tpa)_2]^{2+}$,[24], and $[Fe_2(\mu\text{-O})Cl_2(tpa)_2]^{2+}$.[25] Strictly speaking, however, the V–O–V moiety of the present complex is not linear (175.3(2)°), resulting in a loss of rigorous centrosymmetry. The above iron(III)–tpa complex has a similar bridging angle of 174.7° while the chromium-

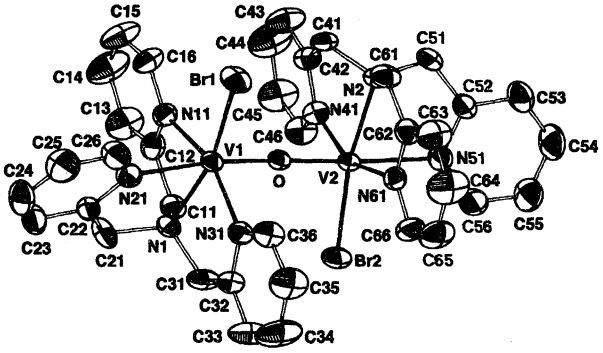

Fig. 6. Perspective view of $[V_2(\mu\text{-O})Br_2(tpa)_2]^{2+}$.

Table 3. Selected Bond Lengths (Å) and Angles (degree) for $[V_2OBr_2(tpa)_2]Br_2 \cdot 2H_2O$

	Bond lengths		
V1–Br1	2.5141(7)	V2–Br2	2.5133(7)
V1–O	1.783(2)	V2–O	1.784(2)
V1–N1	2.133(3)	V2–N2	2.137(3)
V1–N11	2.130(3)	V2–N41	2.131(3)
V1–N21	2.204(3)	V2–N51	2.202(3)
V1–N31	2.114(3)	V2–N61	2.115(3)
	Bond angles		
Br1–V1–O	96.83(8)	Br2–V2–O	96.85(8)
Br1–V1–N1	165.52(7)	Br2–V2–N2	165.55(7)
Br1–V1–N11	97.36(8)	Br2–V2–N41	97.41(9)
Br1–V1–N21	89.14(8)	Br2–V2–N51	89.15(8)
Br1–V1–N31	103.91(9)	Br2–V2–N61	104.05(8)
O–V1–N1	96.7(1)	O–V2–N2	96.7(1)
O–V1–N11	92.1(1)	O–V2–N41	92.2(1)
O–V1–N21	172.8(1)	O–V2–N51	172.8(1)
O–V1–N31	91.8(1)	O–V2–N61	91.9(1)
N1–V1–N11	77.0(1)	N2–V2–N41	77.0(1)
N1–V1–N21	77.8(1)	N2–V2–N51	77.8(1)
N1–V1–N31	80.8(1)	N2–V2–N61	80.6(1)
N11–V1–N21	91.2(1)	N41–V2–N51	91.0(1)
N11–V1–N31	157.8(1)	N41–V2–N61	157.5(1)
N23–V1–N31	82.7(1)	N51–V2–N61	82.7(1)
V1–O–V2	175.3(2)		

(III)– and oxovanadium(IV)–tpa complexes have a linear M–O–M bridge. The lack of rigorous centrosymmetry in the present vanadium(III) complex is also reflected in the mutual arrangement of the tpa ligands as shown in Fig. 7. The monomeric units are mutually rotated around the V–O axis so that one pyridyl ring of a monomeric unit stacks on the counterpart of another monomeric unit.

The dimensions in each monomeric unit are practically the same. The vanadium(III)–oxo distances of the present complex are in the range of those found in other single oxo-bridged vanadium(III) complexes.[21,26—30] The V1–N21 and V2–N51 distances are lengthened due to the trans influence of the bridging oxo atom. The coordination polyhedron around the vanadium(III) center is significantly distorted from a regular octahedron owing to the restricted bite angles of the tpa ligand

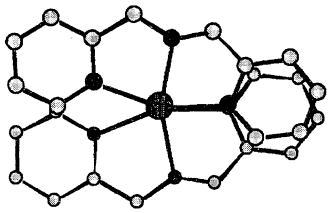

Fig. 7. View of $[V_2(\mu\text{-O})Br_2(tpa)_2]^{2+}$ from the direction of V···V axis. The methylpyridyl groups in the axial positions and bromo ligands are omitted for clarification.

(*cis* N–V–N′ angle ranges 77.0(1)—91.2(1)° and *trans* N–V–N′ angles are ca. 158°).

The electronic and resonance Raman spectra of the tpa complex are typical of oxo-bridged dinuclear vanadium(III) complexes; $LMCT_{max}$=540 nm, $2\times\nu_{as}$(V–O–V)=1324 cm^{-1} (ν_{as}(V–O–V) and ν_s(V–O–V) are obscured by the Raman bands from the tpa ligand).

Correlation between ν_{as}(V–O–V) and the LMCT Maxima. As stated above, the aquation of $[V_2(\mu\text{-O})(bpg)_2Br_2]$ results in a higher-energy shift of $2\times\nu_{as}$(V–O–V) as well as of the LMCT maximum. This observation stimulated us to examine the correlation between $2\times\nu_{as}$(V–O–V) and the LMCT maxima for a series of single-oxo bridged vanadium(III) complexes. As shown in Fig. 8, there is a good linear and positive correlation between $2\times\nu_{as}$(V–O–V) and the LMCT maxima. A similar correlation with the LMCT maxima was also recognized for ν_{as}(V–O–V) and ν_s(V–O–V).

The energy of the M–O–M stretching vibration depends on both the geometry of the M–O–M moiety (namely, the M–O–M angle) and the force constant of the M–μ-O bond. It has been well documented that ν_s(Fe–O–Fe) and ν_{as}(Fe–O–Fe) correlate with the Fe–O–Fe angle for oxo-bridged iron(III) complexes.[31,32] The Fe–O–Fe angle also changes the position of the LMCT transition since it affects the π-bonding character of the Fe(III)–μ-O bond. Holz et al. approved the correlation between ν(Fe–O–Fe) and the energy of the LMCT transition.[32] This correlation has been rationalized as follows. As the M–O–M angle approaches 180°, the π-bonding between the Fe(III) ion and the μ-oxo atom becomes more favorable. The increase in the π-bonding character of the Fe(III)–μ-O bond results in a blue shift of the LMCT transition.

Among the complexes listed in Fig. 8, only two, the tpa and the L-his complexes, have been crystallographically characterized. However, we can reasonably assume that the V–O–V angles for single oxo-bridged vanadium(III) complexes would fall at most in the 150—180° range by referring to the Fe–O–Fe angles of the single oxo-bridged iron(III) complexes.[31] The V–O–V angles of the above two vanadium(III) complexes fall in this range (175.3° for the tpa complex and 153.9° for the L-his complex). It was found that as the Fe–O–Fe an-

gle increases from 155 to 180°, ν_{as}(Fe–O–Fe) increases by ca. 50 cm^{-1}.[31] Although a similar trend can be expected for the vanadium(III) complexes, the change observed in $2\times\nu_{as}$(V–O–V) of the tpa and the L-his complexes is against this expectation. Namely, the tpa complex that has a larger V–O–V angle than the L-his complex shows a ν_{as}(V–O–V) at a lower position (1325 cm^{-1} versus 1437 cm^{-1}). This indicates that in the present vanadium(III) complexes the V–O–V angle is not a predominant origin for the correlation between $2\times\nu_{as}$(V–O–V) and the LMCT maxima. Therefore, we examined the change in the V(III)–μ-O bonding character expected for the other origin of the observed correlation.

On inspecting Fig. 8, we noticed the following facts: (1) The aqua complex occupies the highest energy position. (2) The positions of the aminopolycarboxylato complexes are lower than that of aqua complex and are similar to each other. (3) Coordination of bromide, pyridyl nitrogen, and imidazolyl nitrogen decreases the energy of the V–O–V stretching and the LMCT transition. Especially, bromide coordination affects them to a significant extent. It appears from these facts that the greater the softness of the coexisting ligands, the lower the energy of the V–O–V stretching and the LMCT transition. The increase of the softness of the coexisting ligands would decrease the hardness of the vanadium(III) center. Since the bridging oxo atom is a typical hard base that prefers bonding with a hard acid and a harder acid acts as a better π-bond acceptor, a decrease in the hardness of the vanadium(III) center would be unfavorable for the covalency (including π-bonding) of the V(III)–μ-O bond. Then, the LMCT transition is expected to exhibit a red shift due to the decrease in the π-bonding character, based on the same argument presented by Solomon et al.[33] The decrease in the covalent character of the V(III)–μ-O bond should result in a decrease of the force constant of the V(III)–μ-O stretching vibration and, therefore, a decrease in ν_{as}(V–O–V). Thereby, a positive correlation can be expected between the energy of the LMCT transition and ν_{as}(V–O–V).

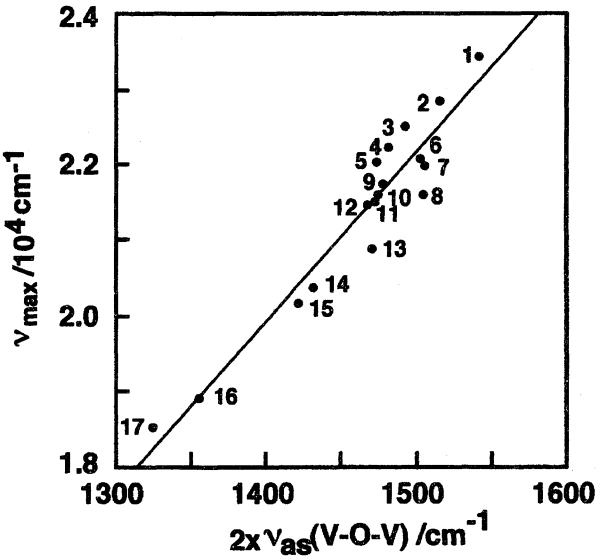

Fig. 8. Correlation between the $2\times\nu_{as}$(V–O–V) and the LMCT maxima: 1, aqua complex in solution;[a] 2, 1,2-diaminoethane-*N*,*N*′-diacetate (edda) complex in solution;[b] 3, nitrilopropionatediacetate (β-alada) complex in solution;[b] 4, 1,2-diamonoethane-*N*,*N*′-disuccinate (edds) complex in solution;[c] 5, nitriloacetatedipropionate complex in solution;[b] 6, triethylenetetraminehexaacetate (ttha) complex in solution;[a] 7, *N*-ethyl-1,2-diaminoethane-*N*,*N*′,*N*′-triacetate (eed3a) complex in solution;[c] 8, the pda complex in solid state;[d] 9, 1,2-diaminoethane-*N*,*N*′-diacetate-*N*,*N*′-dipropionate (eddda) complex in solution;[c] 10, 1,3-diaminopropane-*N*,*N*,*N*′,*N*′-tetraacetate (1,3-pdta) complex in solution;[c] 11, tris(2-pyridylmethyl)-1,4,7-triazacyclononane (tptcn) complex in solution;[b] 12, 1,3-diaminopropane-*N*,*N*′-disuccinate (pdds) complex in solid state;[b] 13, the bpg complex in aqueous solution;[d] 14, L-histidinate complex in solid state;[e] 15, *N*,*N*′-bis(2-pyridylmethyl)-1,2-diaminoethane (bispicen) in solution;[b] 16, the bpg complex in solid state;[d] 17, the tpa complex in solid state.[d] a) Ref. 20, b) unpublished results, c) Ref. 18, d) present work, e) Ref. 21.

In summary, the energy of the M–O–M stretching vibration depends on both the M–O–M angle and the force constant of the M–O bond. For the iron(III) complexes, the correlation between ν_s(Fe–O–Fe) and the LMCT maxima were examined for $[Fe_2(\mu\text{-O})(tpa)_2(L)]$ complexes, where L is a carboxylate or an oxoacidate.[32] In this case, the change in the Fe(III)–μ-O bonding character induced by the coexisting ligands would be small. Then, the Fe–O–Fe angle would play a major role in the change of the Fe–O–Fe stretching vibration. On the contrary, since the change in the V–O–V angle is expected to be rather small for the present single oxo-bridged vanadium(III) complexes, the energy of the V–O–V stretching vibration would correlate primarily to the V(III)–μ-O bonding character.

Magnetic Properties of $[V_2(\mu\text{-O})Br_2(tpa)_2]Br_2$. The temperature-dependent magnetic susceptibility has been studied for several single oxo-bridged dinuclear vanadium(III) complexes.[28,29] Very strong ferromagnetic spin exchange coupling was observed for these complexes. Figure 9 shows the magnetic susceptibility and the effective magnetic moment of $[V_2(\mu\text{-O})Br_2(tpa)_2]Br_2$ as a function of temperature. The magnetic moment per vanadium at room temperature is 3.22 μB, which is larger than the spin-only value of 2.83 μB for an octahedral vanadium(III) complex. The observed magnetic behavior is very similar to earlier results.[28,29]

It has been noted that the μ-oxo dinuclear vanadium(III) complexes exhibit strong ferromagnetic coupling while the μ-oxo complexes of other early transition metals such as Ti(III), Cr(III), Mn(III), and Fe(III) show

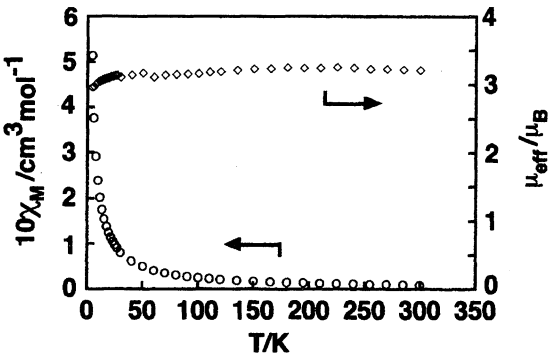

Fig. 9. Plot of the magnetic suceptibility and the effective magnetic moment against temperature for $[V_2(\mu\text{-}O)Br_2(tpa)_2]Br_2 \cdot 2H_2O$.

antiferromagnetic coupling. Recently, Hotzelmann et al. gave an explanation for the puzzling results of the V(III)–O–V(III) systems based on the molecular orbital treatment.[34] Fink et al. discussed the magnetic exchange coupling in the linear oxo-bridged dinuclear complexes of Ti(III), V(III), and Cr(III) on the basis of ab initio calculations.[35] However, it does not seem to be fully understood why the V–O–V systems need a mechanism different from those for other M–O–M systems to explain the spin exchange coupling.

In our previous paper,[15] we showed that in the LMCT excited state the molecular structure of the μ-oxo dinuclear vanadium(III) complexes may be distorted unsymmetrically on the basis of the resonance Raman behavior. This situation is different from that of the iron(III) complexes that would be expected to be distorted symmetrically in the CT excited state. We are now examining if this difference in the molecular structure in the low energy LMCT excited state could explain the difference in the spin-exchange coupling behavior between the oxo-bridged vanadium(III) and iron(III) complexes.

We are grateful to Professor Yosikazu Isikawa of Toyama University for the magnetic susceptibility measurements. We also thank Professors Junjiro Kanamori, Kizashi Yamaguchi, and Wasuke Mori (Osaka University) for their useful discussions about the magnetic properties of $[V_2(\mu\text{-}O)Br_2(tpa)_2]Br_2$.

References

1) H. Michibata and H. Sakurai, "Vanadium in Biological Systems," ed by N. D. Chasteen, Kluwer Acad. Publ., the Netherlands (1990), pp. 153—171.

2) R. Wever and K. Kustin, *Adv. Inorg. Chem.*, **35**, 81 (1990).

3) T. Ishii, I. Nakai, C. Numako, K. Okoshi, and T. Otake, *Naturwissenshaften*, **80**, 268 (1993).

4) M. Henze, *Hoppe-Seyler's Z. Physiol. Chem.*, **72**, 494 (1911).

5) E. Boeri and A. Ehrenberg, *Arch. Biochem. Physiol.*, **50**, 404 (1954).

6) D. H. Anderson and J. H. Swinehart, *Comp. Biochem. Physiol., Part A*, **99A**, 585 (1991).

7) E. Kime-Hunt, K. Spartallion, S. Holmes, M. Mohan, and C. J. Carrano, *J. Inorg. Biochem.*, **41**, 125 (1991).

8) Y. Nishida, A. Goto, T. Akamatsu, S. Ohba, T. Fujita, T. Tokii, and S. Okada, *Chem. Lett.*, **1994**, 641.

9) S. Ménage and L. Que, Jr., *New J. Chem.*, **15**, 431 (1991).

10) S. Kojima, K. Okazaki, S. Ooi, and K. Saito, *Inorg. Chem.*, **22**, 1168 (1983).

11) M. Suzuki, H. Senda, Y. Kobayashi, H. Oshio, and A. Uehara, *Chem. Lett.*, **1988**, 1863.

12) For example: L. Que, Jr., and A. E. True, *Progr. Inorg. Chem.*, **38**, 97 (1990).

13) G. Anderegg and F. Wenk, *Helv. Chim. Acta*, **50**, 2330 (1967).

14) D. D. Cox, S. J. Benkovic, L. M. Bloom, F. C. Bradley, M. J. Nelson, L. Que, Jr., and D. E. Wallick, *J. Am. Chem. Soc.*, **110**, 2026 (1988).

15) K. Kanamori, K. Ino, H. Maeda, K. Miyazaki, M. Fukagawa, J. Kumada, T. Eguchi, and K. Okamoto, *Inorg. Chem.*, **33**, 5547 (1994).

16) "Enraf- Nonius Structure Determination Package (SDP)," Enraf–Nonius, Delft, The Netherlands (1978).

17) C. K. Fair, "MOLEN, International Structure Solution Procedure," Enruf–Nonius, Delft, the Netherlands (1990).

18) K. Okamoto, J. Hidaka, M. Fukagawa, and K. Kanamori, *Acta Crystallogr., Sect. C*, **C48**, 1025 (1992).

19) J. C. Robles, Y. Matsuzaka, S. Inomata, M. Shimoi, W. Mori, and H. Ogino, *Inorg. Chem.*, **32**, 13 (1993).

20) K. Kanamori, Y. Ookubo, K. Ino, K. Kawai, and H. Michibata, *Inorg. Chem.*, **30**, 3832 (1991).

21) K. Kanamori, M. Teraoka, H. Maeda, and K. Okamoto, *Chem. Lett.*, **1993**, 1731.

22) R. J. H. Clark and C. S. Williams, *Inorg. Chem.*, **4**, 350 (1965).

23) B. G. Gafford, R. A. Holwerda, H. J. Schugar, and J. A. Potenza, *Inorg. Chem.*, **27**, 1128 (1988).

24) H. Toftlund, S. Larsen, and K. S. Murray, *Inorg. Chem.*, **30**, 3964 (1991).

25) A. Hazell, K. B. Jensen, C. J. McKenzie, and H. Toftlund, *Inorg. Chem.*, **33**, 3127 (1994).

26) P. Chandrasekhar and P. H. Bird, *Inorg. Chem.*, **23**, 3677 (1984).

27) J. K. Money, K. Folting, J. C. Huffmann, and G. Christou, *Inorg. Chem.*, **26**, 944 (1987).

28) S. G. Brand, N. Edelstein, C. J. Hawkins, G. Shalimoff, M. R. Snow, and E. R. J. Tiekink, *Inorg. Chem.*, **29**, 434 (1990).

29) P. Knopp, K. Wieghardt, B. Nuber, J. Weiss, and W. S. Sheldrick, *Inorg. Chem.*, **29**, 363 (1990).

30) Y. Zhang and R. H. Holm, *Inorg. Chem.*, **29**, 911 (1990).

31) J. Sanders-Loehr, W. D. Wheeler, A. K. Shiemko, B. A. Averill, and T. M. Loehr, *J. Am. Chem. Soc.*, **111**, 8084 (1989).

32) R. C. Holz, T. E. Elgren, L. L. Pearce, J. H. Zhang, C. J. O'Connor, and L. Que, Jr., *Inorg. Chem.*, **32**, 5844 (1993).

33) R. C. Reem, J. M. McCormick, D. E. Richardson, F. J. Devlin, P. J. Stephens, R. L. Musselman, and E. I.

Solomon, *J. Am. Chem. Soc.*, **111**, 4688 (1989).
34) R. Hotzelmann, K. Wieghardt, U. Flörke, H. Haupt, D. C. Weatherburn, J. Bonvoison, G. Blondin, and J. Girerd, *J. Am. Chem. Soc.*, **114**, 1681 (1992).
35) K. Fink, R. Fink, and V. Staemmler, *Inorg. Chem.*, **33**, 6219 (1994).